Phase transition of solid bismuth under high pressure*

Hai-Yan Chen(陈海燕)[1], Shi-Kai Xiang(向士凯)[1,†], Xiao-Zhen Yan(颜小珍)[1], Li-Rong Zheng(郑黎荣)[2], Yi Zhang(张毅)[1], Sheng-Gang Liu(刘盛刚)[1], and Yan Bi(毕延)[1]

[1] *National Key Laboratory of Shock Wave and Detonation Physics, Institute of Fluid Physics, Mianyang* 621900, *China*
[2] *Institute of High Energy Physics, Chinese Academy of Sciences, Beijing* 100049, *China*

(Received 22 March 2016; revised manuscript received 5 June 2016; published online 25 August 2016)

As a widely used pressure calibrator, the structural phase transitions of bismuth from phase I, to phase II, to phase III, and then to phase V with increasing pressure at 300 K have been widely confirmed. However, there are different structural versions for phase III, most of which are determined by x-ray diffraction (XRD) technology. Using x-ray absorption fine structure (XAFS) measurements combined with *ab initio* calculations, we show that the proposed incommensurate composite structure of bismuth of the three configurations is the best option. An abnormal continuous increase of the nearest-neighbor distance of phase III with elevated pressure is also observed. The electronic structure transformation from semimetal to metal is responsible for the complex behavior of structure transformation.

Keywords: Bi, phase transition, pressure, XAFS

PACS: 81.30.Bx, 61.50.Ks, 61.05.cj **DOI:** 10.1088/1674-1056/25/10/108103

1. Introduction

Bismuth (Bi) is one of the most studied elements under high pressure due to its peculiar electronic character and its abundance of pressure-induced polymorphic phases. A generally accepted phase-transition sequence with increasing pressure at room temperature is I→ II→ III→ V.[1–5] The phase at ambient pressure (phase I) is of a rhombohedral A7-type structure of space group $R\bar{3}m$.[6] It transforms at 2.55 GPa[7] to phase II exhibiting a monocline structure, which is stable only in a very narrow pressure range, and the second phase transition occurs as the pressure increases to 2.7 GPa.[8] These two phase transitions are widely used as pressure calibration points.[9] The last phase transition, from phase III to phase V occurs at 7.7 GPa.[10] Phase V is characterized by a body centered cubic (bcc) structure shown to be stable to at least 220 GPa.[11]

However, there are still several outstanding uncertainties over the Bi phase diagram, particularly regarding the pressure range from 2.7 GPa to 7.7 GPa (the stability field of phase III). Some studies have found that two additional phase transitions happen at 4.3 GPa and 5.3 GPa.[12,13] In addition, due to the complexity of the diffraction patterns of phase III and the difficulty in indexing these diffraction patterns, the crystal structure of phase III has been differently described during the past 50 years. Three different structures (monoclinic,[14] tetragonal,[15] and orthorhombic[16]) were proposed in the 1970s, but the structures were not convincingly fitted to the experimental data. In the 1990s, Chen *et al.*[17] presented another tetragonal structure which showed a good fit to the phase III XRD peak positions. Recently, Mcmahon *et al.*[3,18] described a structure of a body-centered tetragonal (bct) "host" and an interpenetrating bct "guest" component, which was incommensurate with the host along the *c* axis. This structure is also consistent with the experimental data and shows better coherence in the volume change rate during the phase transition from II to III.

To address the above problem the conflicting structures are produced by the different diffraction experiments, an independent XRD experiment is carried out in this work. To complement those experiments, we also use XAFS spectroscopy, a powerful tool to determine the geometric structure by providing the coordination information within a few angstroms of the absorbing atom.[19] We use XAFS measurements combined with *ab initio* calculations to investigate the phase transitions of bismuth at pressures up to 20 GPa and room temperature. The sequence of phase transitions and the pressure range of each phase are determined, and the most likely crystal structure of phase III is tested. We propose the probable mechanism of an abnormal increase of the nearest-neighbor distance of phase III upon compression, and investigate the electronic structure transition.

2. Experimental and calculation method

The Bi *L*3-edge XAFS spectra of bismuth under different pressures have no diffraction peak in an energy range from −200 eV to 450 eV relative to the edge energy (13.404 keV),

*Project supported by the National Natural Science Foundation of China (Grant Nos. 10904133, 11304294, 11274281, 11404006, and U1230201), the Development Foundation of China Academy of Engineering Physics (Grant Nos. 2015B0101004, 2013B0401062, and 2012A0101001), the Research Foundation of the Laboratory of Shock Wave and Detonation, China (Grant No. 9140C670201140C67282).

†Corresponding author. E-mail: skxiang@caep.cn

© 2016 Chinese Physical Society and IOP Publishing Ltd

which were measured at the EXAFS beamline 1W1B at the Beijing Synchrotron Radiation Facility (BSRF) with the transmission mode. Up to 20 GPa pressure scenario was generated by a diamond anvil cell (DAC) with a pair of monocrystalline conical diamonds of 200-μm flat culet. The ruby R1 fluorescence technique was used to measure the pressure. A T301 gasket was compressed to 30 μm and a ∼ 70-μm diameter hole was drilled in the center. The hole was filled with polycrystalline Bi sample of 99.998% purity (Alfa Aesar Co.) and a small sphere of ruby for pressure measurement. Because bismuth is relatively soft under high pressure, no pressure-transmitting medium was used in these experiments. Single-crystal diffraction of diamond, which would be superposed onto the XAFS spectra as drastic interference signal, was suppressed by rotating the DAC to adjust the angle between the DAC orientation and the incident x-ray. To obtain the EXAFS oscillations $k^2\chi(k)$ and the radial structural functions (Fig. 1) from the XAFS raw data, the ATHENA software[20] was used. The calculated XANES spectra were obtained by using the FDMNES code,[21] in multiple scattering mode and with X-alpha exchange–correlation potential.[22]

The powder diffraction data were collected on the station 4W2 specifically designed for high-pressure physics at the BSRF using the Mar345 image-plating detector. Monochromatic x-ray was used as the incident illumination with a wavelength of 0.61992 Å. Mean current of the beam was about 250 mA, and the size of the facula was 14 μm×35 μm. The pressure was created by DAC and calibrated by the fluorescence peak position of ruby. The same sample was loaded into a 200-μm diameter hole with a thickness of 40 μm that was drilled in a T301 gasket.

To optimize the structures and calculate the electronic properties of Bi, we applied the density functional theory in the framework of the projector augmented wave (PAW)[23] method as implemented in the code VASP (Vienna *ab initio* simulation package).[24] The exchange–correlation potential was approximated by generalized gradient approximation (GGA) using Perdew–Burke–Ernzerhof (PBE) functional.[25] To ensure convergence (< 1 meV/atom), the kinetic cutoff energy of 450 eV, and Monkhorst–Pack k-meshes[26] with grid spacings of 0.2 Å^{-1} and 0.1 Å^{-1}, were chosen for structural optimizations and calculations of electronic density of states, respectively.

3. Results and discussion

Figure 1(a) shows the pressure dependences of Bi $L3$-edge EXAFS oscillations $k^2\chi(k)$ at 300 K, in which k^2 is a weighting factor used to enhance the amplitude of the data in the region showing high k. The spectra can be divided into four EXAFS oscillation curve groups, highlighted using arrows and dashed lines. Each group of spectra with unique features primarily represents one phase. The radial structural functions, which were Fourier transformed from $k^2\chi(k)$, are shown in Fig. 1(b) and are correspondingly divided into four groups. The dashed-dotted lines are located at the peaks corresponding to the first coordination shell of bismuth under different pressures and indicate the discontinuous changes among the different groups.

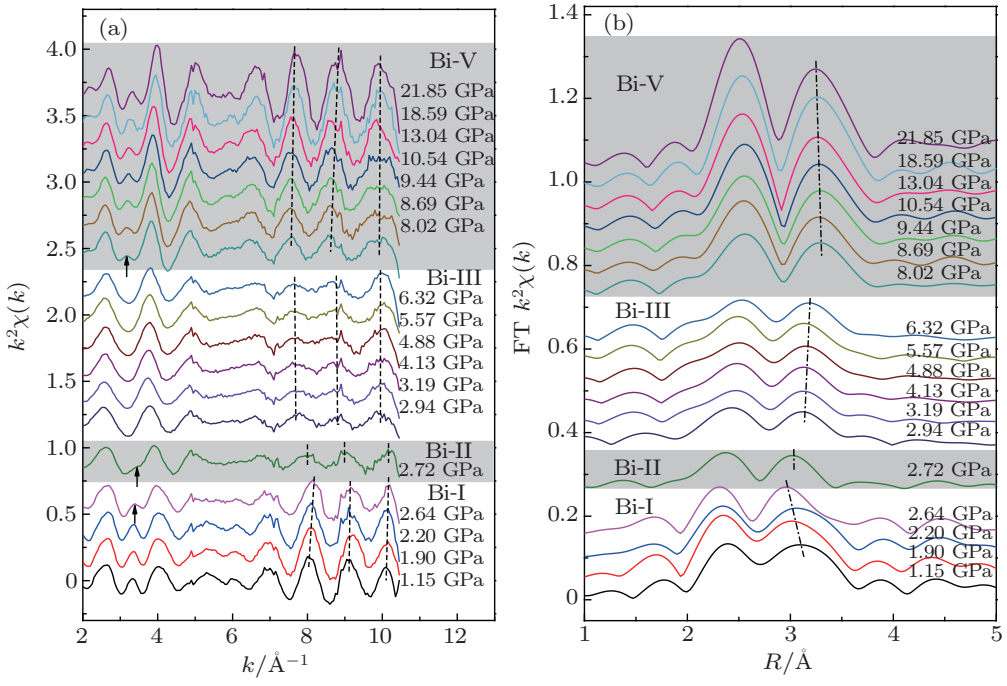


Fig. 1. (color online) Pressure dependences of Bi $L3$-edge EXAFS oscillations $k^2\chi(k)$ (a) and their Fourier transformations (FT) (b) at 300 K. The dark and light blocks divide the curves into different groups. The arrows, the dashed lines, and the dashed-dotted lines highlight the discontinuous changes among the different curve groups.

Comparing with the phase diagram of bismuth (see Fig. 2), we can separate the four groups into phases I, II, III, and V. The phase transitions at 4.3 GPa (III→III′) and 5.3 GPa (III′ →III″) that are plotted with dashed lines in the phase diagram (Fig. 2) are not observed in this experiment, consistent with the previous XRD results. This consistency further proves that there are no structure changes at 4.3 GPa nor at 5.3 GPa, and the anomaly observed in volume[12] and electrical resistance[13] under these pressure points may be associated with the second-order phase transitions. The pressure of the phase transition from phase I to II is about 2.64 GPa∼2.72 GPa based on the EXAFS oscillation curves. This range slightly deviates from the previous experimental results (e.g. Ref. [7]) of 2.55 GPa. This difference might be caused by the difference between the nominal pressure estimated by the fluorescence peak of the ruby embedded in the sample under non-ideal hydrostatic pressure, and the actual pressure. The consistency of phase-transition pressures between our EXAFS results and those of previous studies indicates that XAFS can provide an independent, complementary approach to studying the phase transition of Bi.

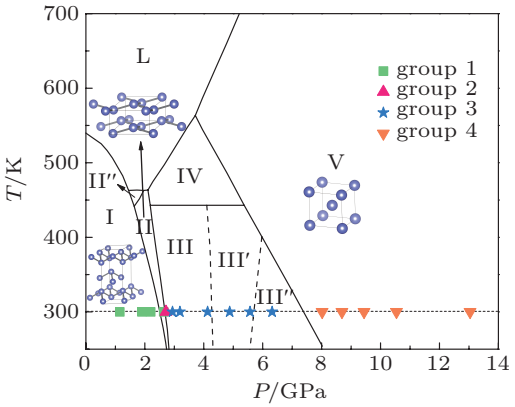


Fig. 2. (color online) Pressure–temperature phase diagram[1–4] of bismuth and the crystal structures of phases I, II, and V. The squares, the triangles, the stars, and the upside-down triangles represent the pressure points measured in this work which are divided into 4 groups.

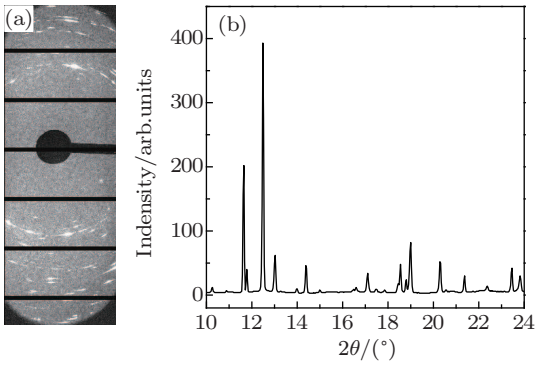


Fig. 3. XRD image (a) and the integrated one-dimensional (1D) profile (b) of Phase III under 4.3 GPa.

Given the different XRD experimental data for phase III, we also independently performed several XRD experiments by using polycrystal Bi powder. The XRD image of phase III at 4.3 GPa and its integrated profile are shown in Fig. 3. Applying single crystal diffraction and low temperature technology, a recent report[3] described a set of clear lines of diffuse scattering in the XRD patterns and a new incommensurate host-guest structure of phase III was proposed. In our work, these diffuse scattering lines in the two-dimensional (2D) image are not observed (Fig. 3(a)). Obviously, the structure of phase III is hard to detect by using x-ray powder diffraction.

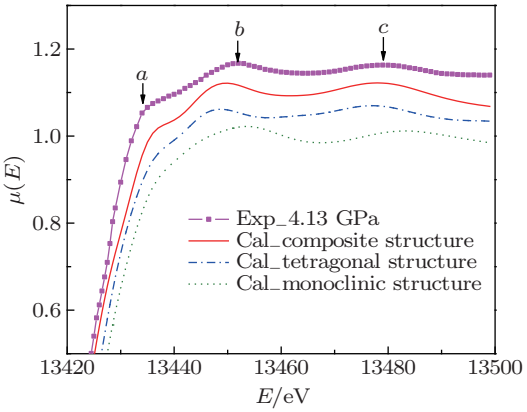


Fig. 4. (color online) Comparisons between the experimental XANES spectrum and the calculated spectra of phase III. The crystal structures for calculating the spectra are cited from Ref. [4] (solid line), Ref. [15] (dashed-dotted line), and Ref. [12] (dotted line).

Due to the lack of novel structural information from our XRD measurements, we use XAFS to determine whether the evidence could be found for any of the structures of phase III previously described, including the monoclinic structure,[14] the tetragonal structure[17] and the incommensurate composite host–guest structure.[3] The structures proposed by Duggin[15] and Fedotv *et al.*[16] in the early 1970s are not discussed in this work due to the absence of detailed atomic positional parameters. Figure 4 shows the comparisons between the experimental XANES spectrum of phase III collected at 4.13 GPa and the calculated spectra based on the three different crystal structures. Because of the lack of ideal periodicity for the incommensurate host–guest structure, it is impossible to set a supercell to reproduce the structure exactly by calculations. Instead, we use an approximate structure based on $c_{\mathrm{H}} : c_{\mathrm{G}} = 4 : 3$ (here the subscripts H and G represent the host and guest, respectively) for the incommensurate composite structure. The lattice parameters of the unit cell are $a = 8.5182$ and $c = 12.4926$, and the new symmetry space group $P4/mcc$ (shown in Fig. 5). In a range of 0 eV–80 eV relative to the edge energy, the experimental spectrum (Fig. 4) exhibits a plateau "*a*" between 13.434 eV and 13.444 eV and two peaks "*b*" and "*c*" located at 13.452 eV and 13.479 eV, respectively. The plateau "*a*" fully merges together with "*b*" in the spectrum calculated for the monocline structure. Additionally, in comparison to the other two calculated spectra, the locations of peaks "*b*" and "*c*" in the spectrum calculated with the composite structure are closest to the experimental data. Therefore the composite structure

is the most consistent with the data in all three structures.

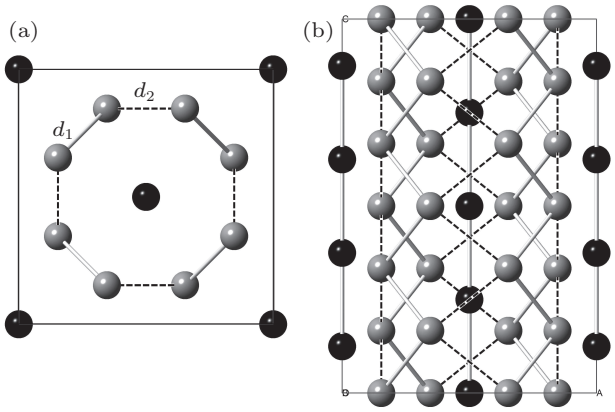


Fig. 5. $P4/mcc$ phase III model structure along [001] (a) and [010] (b). The host atoms are shown as gray spheres while the guest atoms are shown as black ones. The gray cylinders denote the shortest distances within the host (zigzag chains) and within the guest (linear chains). The second-neighbor distances are outlined using dashed lines.

Next, the enthalpies each as a function of pressure for these three structures are calculated. All enthalpies are referenced to the composite structure ($\Delta H = H - H_{\text{Composite}}$) as shown in Fig. 6. The enthalpy of the composite structure is the lowest in a pressure range of 0 GPa–10 GPa (the pressure range of phase III is 2.7 GPa–7.7 GPa in fact). Therefore, the reported incommensurate composite structure is the most reasonable structure of phase III.

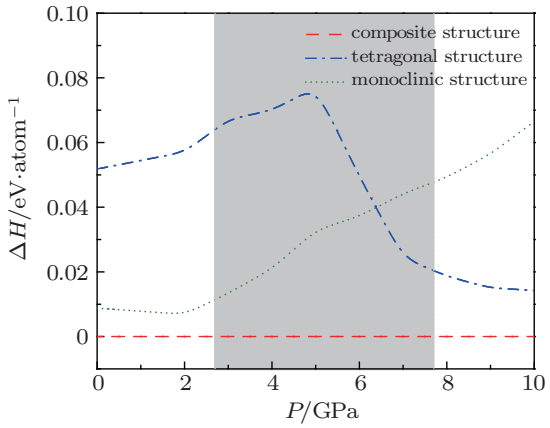


Fig. 6. (color online) Enthalpies each as a function of pressure for the three different phase III structures. All enthalpies are referenced to the composite structure ($\Delta H = H - H_{\text{Composite}}$). The structures are cited from Ref. [4] (dashed line), Ref. [15] (dashed-dotted line), and Ref. [12] (dotted line).

The XAFS spectra are divided into four groups representing phases I, II, III, and V, and figure 7(a) shows the experimental Bi$L3$-edge XANES spectra of the four phases. The spectra measured under 1.15 GPa, 2.72 GPa, 4.13 GPa, and 8.02 GPa are selected from each group as example spectra for the four phases. The spectrum of phase I shows a plateau "A" , a major peak "B" and two peaks "C" and "D" (Fig. 7(a)). During the three phase transitions, the plateau "A" flattens while the major peak "B" is basically unchanged. Peak "C" dramatically decreases from phase I to phase II transition, and disappears in the curve of phase III, but finally reappears in the curve of phase V. Peak "D" shifts to the lower energy in the first two phase transitions and slightly moves back to the high energy in the last phase transition. Bump "E" only occurs in the spectrum of phase V.

The calculated XANES spectra based on the structures of I (rhombohedral), II (monoclinic), III (incommensurate composite host–guest), and V (bcc) are displayed in Fig. 7(b), respectively. Since the spectrum of phase II is quite different from the experimental results, the spectra of the mixtures of pure II with I or III (shown in the inset of Fig. 7(b)) are calculated. Only the curve of the mixture of II and I shows peak "C". Using this spectrum of the mixture to replace the one of the pure II curves, the simulated trends of the energy positions and relative intensities for "A–E" of the four phases are in excellent consistence with the experimental results, indicating that the models including the incommensurate composite structure are suitable for the data. The sample is the mixture of II and I under 2.72 GPa and may be affected by the non-ideal hydrostatic pressure.

Using the data shown in Fig. 1(b), the changes in the first-neighbor distance of Bi with increasing pressure can be qualitatively assessed. In the pressure ranges in which phase I and phase V can be stable, the first peaks denoted by the dashed-dotted lines in Fig. 1(b) move towards the lower R direction upon compression due to the contracted first shell. However, the peak of phase III shows a slightly continuous positive shift in its R position, which means that the nearest-neighbor distance of phase III is abnormally lengthened under compression. This phenomenon has not been described in previous XRD experiments. As shown in Fig. 5, the nearest-neighbor bond (d_1) of about 3.1 Å is a bit shorter than the second-neighbor bond (d_2) of over 3.3 Å, suggesting that there are some covalence characteristics in d_1. Supposing that the bonds with the guest along the c axis are extended under compression, this would contradict the XRD experimental result,[27] which suggests that the c axis of the host–guest structure is contracted. Therefore the increase in the nearest-neighbor distance must come from the expansion of the bond within the host. The anomalous expansion of d_1 may correspond to the highly anisotropic covalent state of the incommensurate structure. Under increasing pressure, to reduce the anisotropy, the arrangement of the atoms in the space becomes more uniform, resulting in the weakening of the covalent bond and the expansion of d_1. Similar abnormal changes have been reported in some highly anisotropic liquids.[28–30] Furthermore, it is observed that at each phase transition point, there is a sudden increase of the nearest-neighbor distance, which usually appears in a phase transition from molecular to atomic structure.[31] This is in consistence with the known crystal structure of each phase and implies the decreasing of covalence of Bi with increasing pressure.

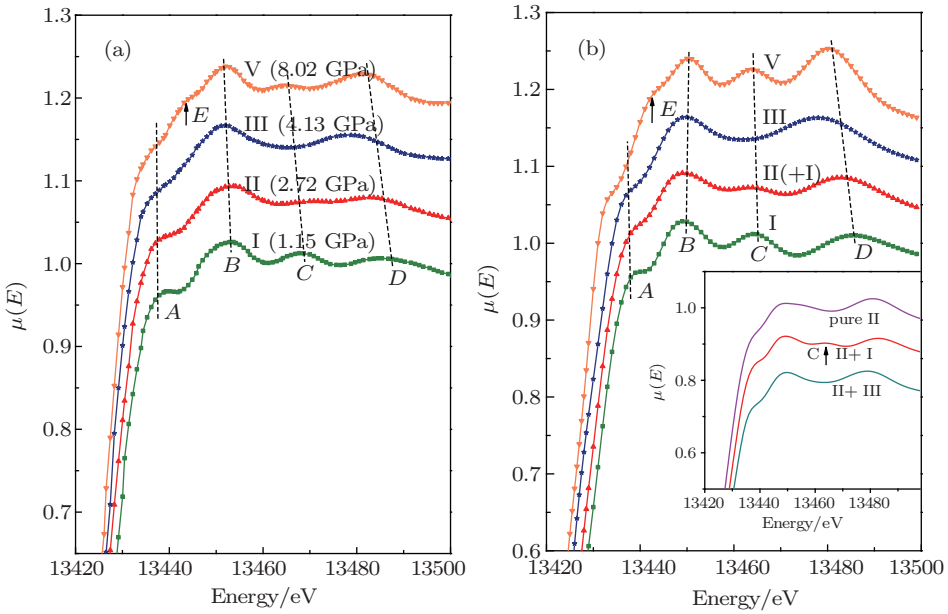


Fig. 7. (color online) Experimental (a) and the calculated (b) Bi $L3$-edge XANES spectra of the four phases. The insert shows the calculated spectra of pure II and the mixtures of pure II with I or III.

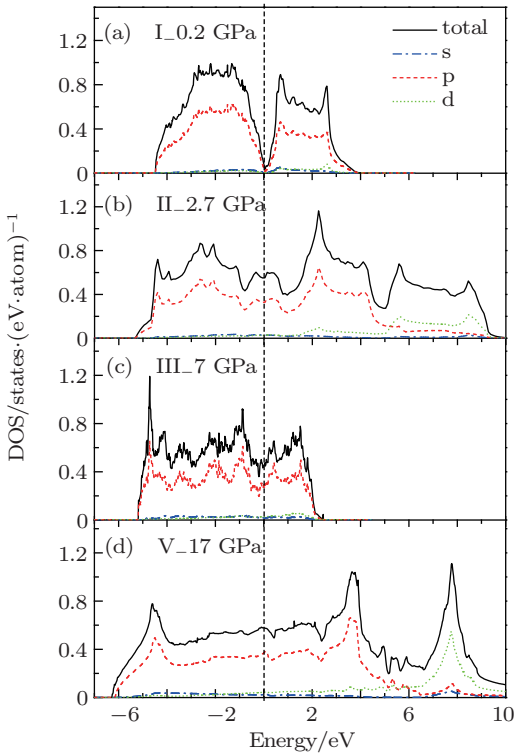


Fig. 8. (color online) Variations of total and the partial DOS with energy for phases I (a), II (b), III (c), and V (d) of bismuth subjected to a transition from semimetal to metal under pressure.

To study the electronic structure transition of bismuth with increasing pressure, the total and partial electronic density of states (DOS) of the four phases are calculated and the results are shown in Fig. 8. In Fig. 8(a), the p band splits into two parts and the Fermi level is located in a deep valley in the p band with a very low DOS value (about 0.02 eV). The total DOS of phase I mainly results from p orbital partial contributions to the Bi–Bi bonds in phase I. The low DOS value at Fermi level implies that Bi–Bi bonds show some strong covalence characteristics, which is in accord with the semimetallic behavior of Bi in the ground state. As shown in Figs. 8(b) and 8(c), the DOSs at the Fermi level are significantly increased, but the valley in the p band is still observed. This means that the semimetal–metal transition occurs but the covalent bonding contribution still exists. Finally, for bcc Bi, the DOS attains an approximately parabolical nearly-free-electron distribution (Fig. 8(d)), indicating that the cohesion in phase V results from the metallic bond. Thus, the metallic character of Bi increases with increasing pressure, which is consistent with the changes in the nearest-neighbor distance. All these electronic structure features contribute to its complex structural transition.

4. Conclusions

In this work, we investigate the phase transitions of bismuth with increasing pressure at 300 K using XAFS measurements. The difference between EXAFS oscillation curves shows that the sequence of phase transition of bismuth is I→ II→ III→ V, and neither the phase transition of III→III′ nor that of III′ →III″ were observed. The pressure ranges stable for each phase have good consistence with the previous research results. Combining XAFS with *ab initio* calculation, we show that the incommensurate composite structure is the best option representing phase III. Interestingly, the nearest-neighbor distance of phase III increases under compression, which may be due to the highly anisotropic covalent state of the incommensurate structure. The calculation of DOS shows that the metallic characteristic increases with increasing pressure, which is responsible for its complex structural transition.

Acknowledgement

The authors are grateful to the staff of the 1W1B EXAFS beamline of BSRF for help in XAFS measurements and data analysis. The XRD data were collected at 4W2 high-pressure beamline of BSRF.

References

[1] Klement W Jr, Jayaraman A and Kennedy G C 1963 *Phys. Rev.* **131** 632
[2] Homan C G 1975 *J. Phys. Chem. Solids* **36** 1249
[3] McMahon M I, Degtyareva O and Nelmes R J 2000 *Phys. Rev. Lett.* **85** 4896
[4] Tonkov E Y and Ponyatovsky E G 2004 *Phase transformations of elements under high pressure* (BocaRaton: CRC Press) pp. 148–150
[5] Li Y H, Chang J Z, Li X M, Yu Y Y, Dai C D and Zhang L 2012 *Acta Phys. Sin.* **61** 206203 (in Chinese)
[6] Cucka P and Barrett C S 1962 *Acta Crystallogr.* **15** 865
[7] Brugger R M, Bennion R B and Worlton T G 1967 *Phys. Lett. A* **24** 714
[8] Bundy F P 1958 *Phys. Rev.* **110** 314
[9] Decker D L, Bassett W A, Merrill L, Hall H T and Barnett J D 1972 *J. Phys. Chem. Ref. Data* **1** 773
[10] Aoki K, Fujiwara S and Kusakabe M 1982 *J. Phys. Soc. Jpn.* **51** 3826
[11] Akahama Y, Kawamura H and Singh A K 2002 *J. Appl. Phys.* **92** 5892
[12] Bridgman P W 1935 *Phys. Rev.* **48** 893
[13] Kossowsky R 1966 *Trans. Metall. Soc. AIME* **236** 1746
[14] Kabalkina S S, Kolobyanina T N and Vereshchagin L F 1970 *Sov. Phys. JETP* **31**
[15] Duggin M J 1972 *J. Phys. Chem. Solids* **33** 1267
[16] Fedotov V K, Ponyatovskii E G and Somenkov V 1978 *Fiz. Tverd. Tela* **20** 1088
[17] Chen J H, Iwasaki H and Ktkegawa T 1996 *High Press. Res.* **15** 143
[18] McMahon M I, Degtyareva O, Nelmes R J, van Smaalen S and Palatinus L 2007 *Phys. Rev. B* **75** 184114
[19] Li Y J, Haschaolu W, Song Z Q, Ou Z Q, Tegus O and Ikuo N 2015 *Chin. Phys. B* **24** 086101
[20] Ravel B and Newville M 2005 *J. Synchrotron Radiat.* **12** 537
[21] Bunău O and Joly Y 2009 *J. Phys.: Condens. Matter* **21** 345501
[22] Slater J C 1951 *Phys. Rev.* **81** 385
[23] Blöchl P E 1994 *Phys. Rev. B* **50** 17953
[24] Kresse G and Furthmüller J 1996 *Phys. Rev. B* **54** 11169
[25] Perdew J P, Burke K and Ernzerhof M 1996 *Phys. Rev. Lett.* **77** 3865
[26] Monkhorst H J and Pack J D 1976 *Phys. Rev. B* **13** 5188
[27] Degtyareva O, McMahon M I and Nelmes R J 2004 *High Press. Res.* **24** 319
[28] Funamori N and Tsuji K 2002 *Phys. Rev. Lett.* **88** 255508
[29] Funamori N and Tsuji K 2001 *Phys. Rev. B* **65** 014105
[30] Ohmura S and Shimojo F 2011 *Phys. Rev. B* **83** 134206
[31] Miao M S, Van Doren V E and Martins J L 2003 *Phys. Rev. B* **68** 094106